BIOCHEMISTRY
including biophysical chemistry & molecular biology

Article

pubs.acs.org/biochemistry

Solution Nuclear Magnetic Resonance Structure of the GATase Subunit and Structural Basis of the Interaction between GATase and ATPPase Subunits in a *two-subunit-type* GMPS from *Methanocaldococcus jannaschii*

Rustam Ali,[†] Sanjeev Kumar,[‡] Hemalatha Balaram,[‡] and Siddhartha P. Sarma*[,†]

[†]Molecular Biophysics Unit, Indian Institute of Science, Bangalore 560012, Karnataka, India

[‡]Molecular Biology and Genetics Unit, Jawaharlal Nehru Center for Advanced Scientific Research, Bangalore 560064, Karnataka, India

Supporting Information

ABSTRACT: The solution structure of the monomeric glutamine amidotransferase (GATase) subunit of the *Methanocaldococcus janaschii* (Mj) guanosine monophosphate synthetase (GMPS) has been determined using high-resolution nuclear magnetic resonance methods. Gel filtration chromatography and ^{15}N backbone relaxation studies have shown that the Mj GATase subunit is present in solution as a 21 kDa (188-residue) monomer. The ensemble of 20 lowest-energy structures showed root-mean-square deviations of 0.35 ± 0.06 Å for backbone atoms and 0.8 ± 0.06 Å for all heavy atoms. Furthermore, 99.4% of the backbone dihedral angles are present in the allowed region of the Ramachandran map, indicating the stereochemical quality of the structure. The core of the tertiary structure of the GATase is composed of a seven-stranded mixed β-sheet that is fenced by five α-helices. The Mj GATase is similar in structure to the *Pyrococcus horikoshi* (Ph) GATase subunit. Nuclear magnetic resonance (NMR) chemical shift perturbations and changes in line width were monitored to identify residues on GATase that were responsible for interaction with magnesium and the ATPPase subunit, respectively. These interaction studies showed that a common surface exists for the metal ion binding as well as for the protein−protein interaction. The dissociation constant for the GATase−Mg^{2+} interaction has been found to be ∼1 mM, which implies that interaction is very weak and falls in the fast chemical exchange regime. The GATase−ATPPase interaction, on the other hand, falls in the intermediate chemical exchange regime on the NMR time scale. The implication of this interaction in terms of the regulation of the GATase activity of holo GMPS is discussed.

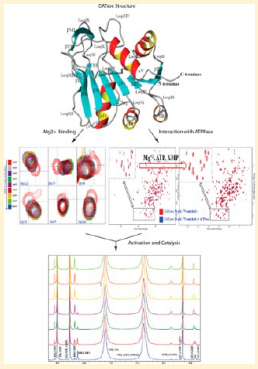

Protein−protein interactions are at the core of most physiological processes.[1−3] Enzymes have evolved to conduct a chemical reaction in an efficient and concerted manner. Guanosine monophosphate synthetase[4] is a special example of a coupled enzyme-catalyzed reaction in which the component reactions are conducted by two distinct domains or subunits. GMPS, a class I glutamine amidotransferase,[5,6] is an important enzyme that catalyzes the final step of GMP biosynthesis. Two reactions are catalyzed by the GMPS enzyme: (1) the hydrolysis of glutamine to yield ammonia and (2) amination of XMP to yield GMP.[7,8] The overall reaction is ATP-dependent and requires Mg^{2+}. The enzyme thus contains two independent catalytic sites that could be housed in individual domains either in a single polypeptide chain or in separate subunits and are known as the GATase and ATPPase domains or subunits. In eukaryotes, bacteria, and some archaea, GMPSs are encoded by a single gene (*two-domain-type*). In most other archaeal species, e.g., *Methanocaldococcus jannaschii*, the GATase and ATPPase functions are present on individual polypeptides (*two-subunit-type*) that are encoded by separate genes. GATase catalyzes the hydrolysis of glutamine and ATPPase uses the ammonia generated to convert XMP to yield GMP. GMP formation occurs via a nucleophilic attack by the released ammonia on the adenyl-XMP intermediate.[9−11]

A Protein Data Bank (PDB) query for GMPS gives 11 hits. All structures have been determined by X-ray crystallography. These structures belong to GMPSs from *Plasmodium falciparum*, *Homo sapiens*, *Thermus thermophilus*, *Coxiella burnetii*, *Pyrococcus horikoshii*, and *Escherichia coli*. Except for *P. horikoshii*, all GMPSs are *two-domain-type*. An analysis of different crystal structures from the PDB reveals that the core structural elements are highly similar in GMPS. The GATase domain or subunit contains α/β structures. The core of the structure is formed by mixed β-sheet mainly constructed from parallel β-strands. The catalytic triad is conserved across these enzymes. The catalytic triad of GATase appears to be similar to those in serine proteases, however, with serine being replaced by cysteine and aspartate by glutamate in GATase.

The ATPPase domain or subunit of GMPS has a typical dinucleotide binding site that resembles that of dehydrogenases. This fold consists of five-stranded sheets sandwiched

Received: April 15, 2013
Revised: May 31, 2013
Published: May 31, 2013

dx.doi.org/10.1021/bi400472e | *Biochemistry* 2013, 52, 4308−4323

between α-helices. ATPPase has a signature nucleotide-binding motif or P-loop that is strongly conserved in all the nucleotide binding proteins.[12] X-ray crystal structures of single-chain GMPSs have shown that the glutamine and XMP binding sites are separated by a distance of 10−40 Å. Thus, the ammonia released at glutamine binding site has to be channeled to the acceptor or ATPPase site.[12−14] Ammonia channeling is the hallmark of a large group of proteins known generally as glutamine-dependent amidotransferases, of which the GMPSs form one subgroup.[7,12,14,15] This ammonia channeling and cross talk between two domains have been a major thrust of the investigation of glutamine amidotransferases. Most of the studies have been conducted on *two-domain-type* GMPS,[12,16−21] while only one study of *two-subunit-type* GMPS has been reported.[22]

The GMPS from *M. jannaschii* is a *two-subunit-type* GMPS. The glutamine amidotransferase (GATase) subunit of *M. jannaschii* is a monomer with a molecular weight of 21 kDa, whereas the ATPPase subunit is a dimer with each protomer having a molecular weight of 34 kDa. There are several open questions with regard to the functioning of this enzyme. Unlike regular enzymes, GATs are bienzymes and therefore function through the formation of protein−protein complexes that is facilitated by binding of ligands to the synthase domain. Further, their activities are tightly coordinated, leading to maximization of the overall catalytic efficiency. Interestingly, different GATs seem to adopt different molecular mechanisms, and thus, the molecular mechanism that coordinates the various events warrants investigation.

Recent studies have shown that the GATase subunit interacts with ATPPase only when the latter is fully liganded, and furthermore, the glutaminase activity is tightly regulated by interaction between GATase and ATPPase subunits.[22] In the case of *M. jannaschii* GMPS, the ATPPase subunit alone is capable of catalyzing the hydrolysis of ATP. On the other hand, the GATase does not show glutaminase activity in the absence of the fully liganded ATPPase subunit. Our interest lies in understanding the structural basis for the interaction between the GATase and ATPPase subunits and the role of this important interaction in catalyzing the formation of GMP. To date, there is no structural information available for the *two-subunit-type* GMPS holoenzyme. Also, poorly understood are the conformational changes in the GATase subunit upon interaction with liganded ATPPase that lead to its activation. To improve our understanding of the mechanistic principles, we initiated structural studies of *M. jannaschii* GMPS. As a first step, we have determined the solution structure of the Mj GATase subunit by high-resolution multinuclear NMR spectroscopy. We have also studied the interaction of GATase with the cofactor Mg^{2+} and the interaction between Mj GATase and the ATPPase subunit.

MATERIALS AND METHODS

Overexpression and Purification. The expression and purification of the Mj GATase subunit of *M. jannaschii* have been described previously.[23] Isotopically enriched (^{13}C, ^{15}N, or ^{15}N) samples of Mj GATase were prepared using [$^{13}C_6$]glucose and $^{15}NH_4Cl$ or $^{15}NH_4Cl$ as the sole sources of carbon and nitrogen, respectively.[24] The gene for the ATPPase subunit from *M. jannaschii* genomic DNA was cloned into pET3atr using NdeI and BamHI restriction sites and subcloned into cassette III of the pST39 expression vector using SacI and KpnI restriction sites. Plasmids carrying the gene for the ATPPase subunit were transformed into the Rosetta (DE3) pLysS *E. coli* overexpression strain. The Mj ATPPase subunit was overexpressed and purified using the same protocol described for the Mj GATase subunit.

Chromatographic Studies. Gel filtration studies were conducted using a Superdex-200 column (10 mm × 300 mm) attached to an AKTA Basic HPLC system. The column was equilibrated with 50 mM phosphate buffer (pH 7.0). β-Amylase (200 kDa), alcohol dehydrogenase (150 kDa), bovine serum albumin (66 kDa), carbonic anhydrase (29 kDa), and cytochrome *c* (12.4 kDa) were used for molecular weight calibration. The protein samples were eluted at a flow rate of 0.5 mL/min.

Gel Filtration Cochromatography. The column was preequilibrated with buffer [20 mM Tris (pH 7.4)] alone or with buffer containing appropriate ligands. The concentrations of ATP and XMP in the running buffer were 100 μM each. The concentrations of Mj ATPPase and GATase when used alone or in combination were 10 μM each. The concentrations of ATP and XMP used for preincubation with the enzyme were 3 and 0.2 mM, respectively. Equimolar Mj GATase and ATPPase were preincubated on ice with substrates under four conditions: (A) 20 mM $MgCl_2$, (B) 20 mM $MgCl_2$ and 3 mM ATP, (C) 20 mM $MgCl_2$ and 200 μM XMP, and (D) 20 mM $MgCl_2$, 3 mM ATP, and 200 μM XMP. These samples were chromatographed. Fractions were collected and analyzed by sodium dodecyl sulfate−polyacrylamide gel electrophoresis (SDS−PAGE).

Metal Affinity Cochromatography. An N-terminal hexahistidine-tagged Mj GATase was generated in pET21b. This clone was verified by DNA sequencing and the protein expressed in Rossetta (DE3) pLysS and purified using Ni-NTA agarose beads. The protein was passed through a desalting column (Sephacryl-200) and concentrated before being used further. Mj GATase affinity beads were generated by incubating Ni-NTA agarose with 10 μM purified Mj GATase followed by a buffer wash to remove the unbound enzyme. Mj ATPPase (10 μM) was incubated for 15 min on ice with 2 mM ATP and 0.2 mM XMP in 20 mM Tris buffer (pH 7.4) containing 20 mM $MgCl_2$. The preincubated Mj ATPPase was mixed with the beads and incubated at 4 °C for 30 min. The beads were then washed with buffer A [20 mM Tris-HCl (pH 7.4)] and subsequently with buffer B [20 mM Tris-HCl (pH 7.4) containing 3 mM ATP, 0.2 mM XMP, and 20 mM $MgCl_2$]. The protein was eluted from the column, using a buffer A solution containing 500 mM imidazole. The column fractions were analyzed by SDS−PAGE.

Biochemical Assay. *Measurement of GATase Activity.* Mj GATase activity was monitored by a coupled enzyme assay in which glutamate formation was coupled to the reduction of NAD^+ to NADH by glutamate dehydrogenase and the reaction was followed by spectrophotometry. The concentration of NADH was estimated from absorbance measurements at 340 nm using a molar extinction coefficient of 6220 M^{-1} cm^{-1}.[25] The reaction mixture consisted of 100 μM GATase and 100 μM glutamine in 100 mM Tris-HCl (pH 7.4) and was incubated at either 22 °C for 30 min or 70 °C for 15 min. The reaction was quenched when the mixture was boiled for 5 min followed by centrifugation at 13000*g*. The supernatant (100 μL) was mixed with 0.5 mM NAD^+ and glutamate dehydrogenase (1.8 units) in a buffer containing 50 mM KCl and 1 mM EDTA. The reaction mixture was incubated for 1 h at 37 °C.

dx.doi.org/10.1021/bi400472e | *Biochemistry* 2013, 52, 4308−4323

Separate control reactions in which GATase and glutamine were mutually excluded were also conducted.

GATase Activity in the Presence of Ligand-Bound ATPPase. The Mj GATase activity was monitored by an assay described in the previous section. Concentrations of enzymes and ligands used in the assays were as follows: 2 μM GATase, 2 μM ATPPase, 0.2 mM XMP, 2 mM ATP, and 5 mM glutamine. Reactions were conducted in a buffer containing 100 mM Tris-HCl (pH 7.4) and 20 mM $MgCl_2$ at 70 °C for 15 min and quenched when the mixtures were boiled for 5 min.

Stoichiometry of the GATase–ATPPase Complex. The stoichiometry of the GATase–ATPPase complex was determined by monitoring the formation of GMP. The reaction mixture contained fixed concentrations of 2 μM ATPPase, 3 mM ATP, 0.2 mM XMP, and 20 mM glutamine and varying concentrations of GATase (0–16 μM). The reaction was conducted in 90 mM Tris-HCl (pH 7.0) containing 20 mM $MgCl_2$ at 70 °C. The reactions were initiated with 2 μM Mj ATPPase and varied concentrations of GATase. Formation of GMP was monitored spectrophotometrically, by measuring the absorbance at 290 nm, and the concentration was estimated using a molar extinction coefficient of 1500 M^{-1} cm^{-1}.[26]

NMR Spectroscopy. *Sample Preparation.* Samples for NMR spectroscopy were prepared in 20 mM potassium phosphate buffer (pH 7.0) containing 2 mM DTT, 0.1 mM EDTA, 1 mM PMSF, and 0.01% sodium azide. Three-dimensional (3D) ^{15}N-edited and ^{13}C-edited NMR experiments were conducted using samples of 0.70 mM Mj GATase in a 90% H_2O/10% D_2O mixture or 100% D_2O. ^{15}N relaxation experiments were conducted using samples of Mj GATase (0.4 mM) in a 90% H_2O/10% D_2O mixture.

Acquisition of Data. NMR data were acquired either on an Agilent 600 MHz spectrometer equipped with a 5 mm triple-resonance pulsed field gradient (TRPFG) probe or on a Bruker Avance 700 MHz spectrometer equipped with a 5 mm TXI triple-resonance PFG (z-axis) probe. The sample temperature was maintained at 30 °C during all experiments. Chemical shifts were referenced to external DSS. Two-dimensional (2D) ^{1}H–^{15}N HSQC spectra[27] were acquired at 700 MHz using proton spectral widths of 14006 Hz in the acquired dimension and 2129 Hz in the indirectly detected dimension. Water suppression was achieved by using a pulse program that incorporated the WATERGATE[28] solvent suppression scheme. The STATES–TPPI mode of quadrature detection was used for frequency selection in the indirectly detected dimension. The ^{1}H–^{13}C HSQC spectra were acquired at 700 MHz in sensitivity-enhanced mode. Proton and carbon spectral widths of 14006 and 10914 Hz, respectively, were recorded in the directly detected and indirectly detected dimensions, respectively. Frequency discrimination in the indirectly detected dimension was achieved via coherence selection using pulsed field gradients. Water suppression was achieved via coherence selection and by the use of trim pulses. Three-dimensional ^{15}N-edited ^{1}H–^{1}H NOESY spectra (mixing times, τ_m, of 150 and 200 ms) and ^{13}C-edited ^{1}H–^{1}H NOESY[29] spectra (mixing time, τ_m, of 150 ms) were acquired at 700 MHz using proton spectral widths of 14005.60 and 14005.60 Hz in the F_3 and F_1 dimensions, respectively, and nitrogen and carbon spectral widths of 2128.65 and 4225 Hz, respectively, in the F_2 dimension. Data were acquired in phase sensitive mode, using the States–TPPI (^{15}N-edited NOESY) or Echo–AntiEcho (^{13}C-edited NOESY) method of quadrature detection for the indirectly detected dimensions.

^{15}N Backbone Dynamics. *Measurement of T_1 and T_2.* The spin–lattice relaxation rate, T_1, and spin–spin relaxation, T_2, were measured by recording two-dimensional ^{1}H–^{15}N HSQC spectra on an Agilent 600 MHz NMR spectrometer equipped with a 5 mm triple-resonance pulsed field gradient (TRPFG) probe.[30,31] The sample concentration used for T_1 and T_2 measurements was 0.4 mM. The data used for T_1 measurement were acquired with 2 s recycle delays and relaxation delays of 10, 50, 100, 250, 400, 550, 750, 900, and 1200 ms. T_2 data were acquired with 2 s recycle delays and relaxation delays of 10, 30, 50, 70, 90, 110, 130, 150, and 170 ms. T_1 and T_2 values were determined by fitting peak heights using the nonlinear least-squares routine, using Analysis.[32]

Calculation of the Rotational Correlation Time (τ_c). The rotational correlation time (τ_c) was measured using the following formula[30,33]

$$\tau_c = 1/4\pi\nu_N(6 \times T_1/T_2 - 7)^{1/2} \quad (1)$$

where ν_N is the ^{15}N resonance frequency (in hertz).

Hydrogen–Deuterium Exchange. A series of 2D ^{1}H–^{15}N HSQC spectra at an interval of 45 min over a period of 24 h were acquired in 100% D_2O. Lyophilized samples of the Mj GATase subunit were dissolved in D_2O just before data were acquired.

Data Processing and Analysis. All 2D and 3D NMR data were processed by using NMRPipe/NMRDraw processing software[34] on an Intel PC workstation running Suse Linux version 11.3. The directly and indirectly detected time domain data of 2D and 3D spectra were processed by applying a 90° phase-shifted squared sine bell or a Gaussian filter with a line broadening parameter of 10 Hz as a weighting function. Data sets were zero-filled prior to Fourier transformation. Processed data were analyzed using the ANALYSIS module in CCPN.

Structure Determination. *Distance and Dihedral Angle Restraints.* Interproton distance restraints were calculated from the intensities of unambiguously assigned NOE correlations in the 3D ^{15}N-edited NOESY-HSQC and ^{13}C-edited NOESY-HSQC spectra. On the basis of integrated intensities, NOEs were classified as strong, medium, weak, and very weak with upper distance bounds of 2.8, 3.5, 5.0, and 6.0 Å, respectively. All distance restraints employed a lower bound of 1.80 Å. Hydrogen bond restraints were generated for residues that were slow to exchange in H–D exchange experiments. The upper distance bounds employed for the hydrogen bonds were set to 2.2 Å for HN···O pairs and 3.2 Å for N···O pairs. Backbone dihedral angles ϕ and ψ were predicted using TALOS^{+35} using the observed H^N, $^1H^\alpha$, $^{13}C^\alpha$, and $^{13}C^\beta$ chemical shifts. An angular variation of ±30° was allowed during structure calculation.

Solution Structure Evaluation. Three-dimensional structures were calculated using the torsion angle dynamics protocol in CYANA version 3.0.[36,37] Experimentally derived distances from NOEs, hydrogen bond distances, and dihedral angle restraints were used as input for the structure calculation. One hundred random conformers were subjected to 20000 steps of annealing. An ensemble of the 20 lowest-energy conformers of 100 calculated conformers were selected on the basis of target function and had no upper distance violations of >0.2 Å or dihedral angle violations of >5°. The conformer with the minimal energy/target function was chosen as a representative conformer. The structures were analyzed using MOLMOL.[38]

The quality of the structure was further assessed by the Protein structure validation suite (PSVS).[39] Structure alignment was performed using either DALI[40] or PyMOL.[41]

Interaction Studies. *Interaction with Cofactor Mg^{2+}.* Perturbations in the chemical shifts of residues in Mj GATase, as observed in $^{1}H-^{15}N$ HSQC spectra, upon interaction with Mg^{2+}, were followed by NMR titration studies. ^{15}N-enriched Mj GATase (50 μM) was titrated with varying concentrations of $MgCl_2$ (0.5−20 mM). The chemical shift perturbation as a function of $MgCl_2$ concentration in the HSQC spectrum was used to calculate the dissociation constant (K_d). The weighted chemical shift change per residue (Δ) was calculated by the equation[42]

$$\Delta = [(\delta_H)^2 + (0.1\delta_N)^2]^{1/2} \quad (2)$$

where δ_H and δ_N are changes in chemical shifts of $^{1}H^{N}$ and ^{15}N, respectively. The dissociation constant for the interaction was determined by plotting Δ as a function of increasing $MgCl_2$ concentration. The resulting curve was fit to the following equation

$$\Delta = \Delta_{max}\{[L]_T + [P]_T + K_d - [([L]_T + [P]_T + K_d)^2 - 4[L]_T[P]_T]^{1/2}\} \quad (3)$$

where Δ is the observed chemical shift change at a given total ligand concentration, $[L]_T$ (relative to the resonance frequency in the absence of $MgCl_2$), Δ_{max} is the change in chemical shift at saturation, and $[P]_T$ is the total protein concentration.[43−47]

Interaction with ATPPase. A method similar to the one described in the previous section was used to study the interaction between Mj GATase and Mj ATPPase subunits. ^{15}N-labeled Mj GATase (50 μM) was titrated with varying concentrations of unlabeled Mj ATPPase (20−160 μM), in the presence of a saturating concentration of all substrates, viz., $MgCl_2$ (20 mM), ATP (8 mM), and XMP (2 mM). All the experiments were conducted in a 40 mM potassium phosphate buffer (pH 7.0) containing 50 mM NaCl. The control experiment was conducted with ^{15}N-enriched Mj GATase (50 μM) in the presence 20 mM $MgCl_2$, 8 mM ATP, and 2 mM XMP. To this was added varying concentrations of unlabeled Mj ATPPase (20− 160 μM). Each titration experiment was started on a freshly prepared sample to avoid a dilution effect upon addition of ligand. All samples were prepared from the same stock solutions. Data were recorded by placing the sample in a 5 mm, deuterium susceptibility matched Shigemi tube. The total sample volume used in a Shigemi tube was kept constant at 300 μL. The concentrations of stock solutions of Mj GATase and Mj ATPPase were 0.43 and 0.53 mM, respectively. The Mj GATase and Mj ATPPase protein concentrations were measured on a NanoDrop 1000 spectrophotometer using molar extinction coefficients of 15930 and 22190 M^{-1} cm^{-1}, respectively. The intensity of a resonance in the control experiment was taken as the reference intensity (I_0). The decrease in intensity due to the line broadening and/or chemical exchange contribution to the relaxation, arising from interaction between two subunits, was determined by measuring the peak height. The change in intensity (ΔI) upon ligand binding was calculated as

$$\Delta I = I_0 - I \quad (4)$$

where I_0 is the peak intensity in the absence of ligands in a control experiment and I represents the peak intensity in the presence of a ligand, analogous to the approach used in ref 48. The data were normalized with respect to reference intensity (I_0). The intensity of a resonance that disappeared on titration with the ATPPase subunit was taken to be zero. The calculated $\Delta I_{normalized}$ was plotted against residue number. A cutoff of 0.8 was set for the residue interacting directly with the Mj ATPPase subunit, while a cutoff of ≥0.75 but <0.8 was set for the residues interacting indirectly. The residues involved in interaction with the Mj ATPPase subunit were mapped onto the calculated solution NMR structure of Mj GATase.

H−D Exchange Studies. To identify interface residues in the Mj GATase−ATPPase complex, H−D exchange NMR experiments were also conducted. The sample for the control experiment was prepared by lyophilization of 50 μM Mj GATase. Equivalent amounts of powdered $MgCl_2$, ATP, and XMP were added, and the mixture was dissolved in D_2O, just prior to data acquisition. The final concentrations of $MgCl_2$, ATP, and XMP in the solution were 20, 8, and 2 mM, respectively. Similarly, Mj GATase (50 μM) and ATPPase (50 μM) were colyophilized, and subsequently, an equivalent amount of the powdered form of $MgCl_2$, ATP, and XMP were added. D_2O was added just before data acquisition. $^{1}H-^{15}N$ HSQC spectra were acquired as described above.

Reaction Assay. All reaction assays were conducted in 20 mM phosphate (pH 7.0) buffer at 303 K. The reaction mixture contained 5 μM Mj GATase, 5 μM Mj ATPPase, 20 mM $MgCl_2$, 2 mM ATP, 240 μM XMP, and 20 mM glutamine. The substrates and cofactors were mixed. The reaction was initiated by the addition of enzymes, and this reaction mixture was transferred into an NMR tube. The time course of the reaction was followed by recording one-dimensional proton NMR spectra. GMP formation was tracked by monitoring the H8, $6NH_2$, and H1′ resonances of GMP, which are known to occur at 8.3, 6.3, and 5.8 ppm, respectively. Chemical shifts were referenced to internal DSS. In a similar manner, formation of AMP was monitored by tracking the H8 resonance of AMP at 8.55 ppm. GATase and glutamine were excluded from the reaction mixture, where only AMP formation was monitored. Spectra were recorded at intervals of 10 min, processed, and analyzed.

RESULTS

Solution Properties of Mj GATase. Figure 1 shows the gel filtration chromatography elution profile when the case in which the Mj GATase subunit is passed through a Superdex-200 gel filtration column. Comparison of the elution volume (V_e) of Mj GATase with those of proteins with known molecular weights showed that Mj GATase behaves as a monomer in solution with a molecular weight of ∼21 kDa. In light of this, the protocols followed for structure determination were those that were generally applicable for monomeric proteins.

NMR Spectroscopy. *Sequence Specific Assignment and Secondary Structure.* Figure 2 shows the sequence specifically assigned $^{1}H-^{15}N$ HSQC spectra of the GATase subunit of Mj GMPS. The sequential connectivity assignments obtained from analysis of the three-dimensional ^{15}N-edited NOESY-HSQC spectrum for residues 35−40 are shown in Figure 3. A summary of the sequential and short-range NOEs between backbone atoms and side chain and backbone atoms is shown in Figure S1 of the Supporting Information. The Mj GATase subunit consists of 11 β-strands and five α-helices. Assignment of sequential, short-range, and medium-range NOEs provided corroborative evidence of the secondary structure determined

dx.doi.org/10.1021/bi400472e | Biochemistry 2013, 52, 4308−4323

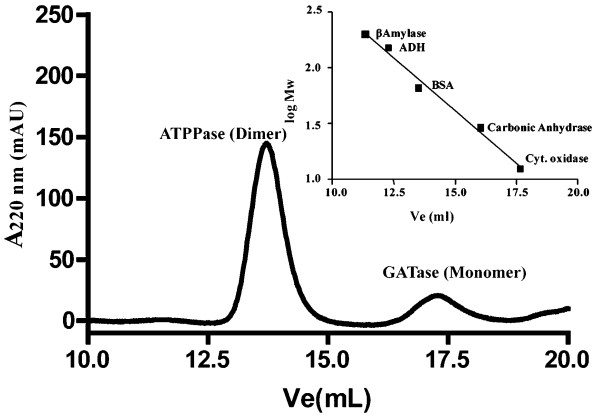

Figure 1. Gel filtration chromatogram showing the elution profile of Mj GATase (monomer) and ATPPase (dimer) on a Superdex-200 column. The inset shows the molecular weight calibration curve obtained using β-amylase, ADH (alcohol dehydrogenase), BSA (bovine serum albumin), carbonic anhydrase, and cytochrome *c* as the molecular weight markers.

from ^{1}H and $^{13}C^{\alpha}$, $^{13}C^{\beta}$ secondary chemical shifts. The distribution of secondary structure as a function of sequence number and its comparison with the secondary structure of the GATase subunit from *P. horikoshii* are listed in Table S1 of the Supporting Information.[23]

Three-Dimensional Structure. The three-dimensional structure of Mj GATase was determined using NMR-derived distance, dihedral, and hydrogen bond restraints. The number and type of restraints used for structure calculation are listed in Table 1. Table 1 also lists the structural parameters derived for the 20 lowest-energy structures. Figure 4a shows the superposition of the 20 lowest-energy conformers of the Mj GATase subunit when superimposed on their backbone (N, C, and C^{α}) atoms. The rmsd values, when superposed on the backbone (N, C, and C^{α}) atoms and on all heavy atoms, with respect to their mean coordinate position, were 0.35 ± 0.06 and 0.8 ± 0.06 Å respectively. An analysis of the backbone dihedral angles in the ensemble of calculated structures shows that 99.4% of backbone dihedral angles are present in the allowed region of the Ramachandran map.[49,50] The low rmsd values for backbone and heavy atoms of all residues (1−188) and the high percentage of residues occupying the allowed regions in the Ramachandran map indicate that the quality of the calculated structure is good. Figure 4b shows the lowest-energy conformer of Mj GATase in ribbon representation. The core of the GATase structure is a mixed β-sheet formed by seven β-strands. This mixed β-sheet consists almost entirely of parallel β-strands, except β-strand XI, which is antiparallel in orientation to both strands IX and X. This arrangement makes the mixed β-sheet appear as though it consists of one β-sheet consisting of five parallel strands and one β-sheet consisting of two antiparallel strands. The first and last β-strands of the core β-sheet are twisted. The core β-sheet is flanked on both sides by five α-helices. The catalytic Cys76 is the only residue with backbone dihedral angles that is present in the disallowed region of the Ramachandran map. This residue is present at the end of a β-strand and beginning of an α-helix. A similar structural feature has been also observed in other α/β-hydrolases[51] (peroxidases, esterases, etc.), where the nucleophilic residue is present in a tight α/β-turn called a "nucleophilic elbow". The presence of this nucleophilic elbow forces the catalytic residue to populate the disallowed region in the Ramachandran map.

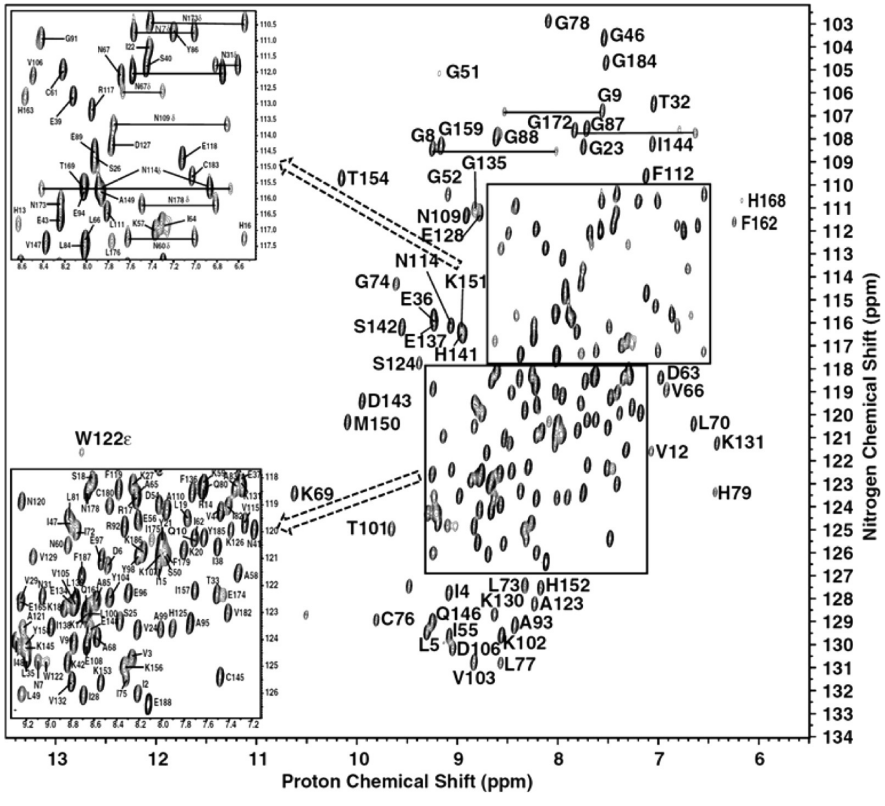

Figure 2. Sequence specifically assigned two-dimensional $^{1}H-^{15}N$ HSQC spectrum of the Mj GATase subunit.

dx.doi.org/10.1021/bi400472e | *Biochemistry* 2013, 52, 4308−4323

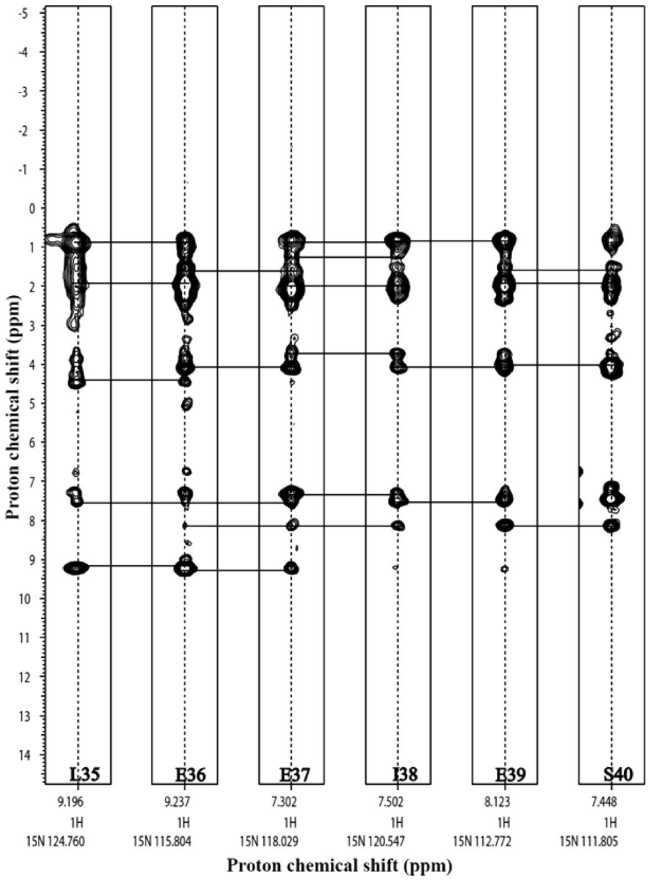

Figure 3. Two-dimensional strip plots from the three-dimensional ^{15}N-edited ^{1}H−^{1}H NOESY-HSQC spectrum of the Mj GATase subunit. Strong sequential backbone HN−HN and H$^{\alpha}$−HN NOE correlations for residues 35−40 indicate that these residues constitute an α-helix. Side chain to backbone NOE correlations are also shown.

Table 1

no. of NOE-based distance restraints	
total	1781
intraresidue ($\|i - j\| = 0$)	670
sequential ($\|i - j\| = 1$)	526
medium-range ($\|i - j\| \leq 4$)	200
long-range ($\|i - j\| \geq 5$)	385
NOE restraints per residue[a]	9.73
no. of hydrogen bond restraints	110
no. of dihedral angle restraints	364
total no. of restraints[a]	2255
total no. of restraints per residue[a]	12.32
total no. of structures calculated	100
no. of structures used	20
no. of restraint violatons[b,c]	
dihedral angle of >5°	0
distance of >0.2 Á	0
van der Waals	3
Ramachandaran plot (Procheck)	
most favored regions (%)	81.6
additionally allowed regions (%)	17.7
generously allowed regions (%)	0.1
total allowed regions (%)	99.4
disallowed regions (%)	0.6
Ramachandaran plot (Richardson's lab)	
most favored regions (%)	92.5
allowed regions (%)	7.0
total allowed regions (%)	99.5
disallowed regions (%)	0.5
rmsd from mean structure coordinate (Å)	
backbone[b]	0.3
average heavy atom[b]	0.8

[a]There are 183 residues with conformationally restricting restraints. [b]Analyzed for residues 1−188. [c]Calculated for all restraints for the given residues, using an average r^{-6}.

Comparison with GATase of P. horikoshii. The GATase subunit of Mj GMPS and that of Ph GMPS are 56% identical in sequence. The distribution of secondary structural elements as a function of sequence in Mj GATase is similar to that observed in the X-ray structure of the GATase subunit of the Ph GMP synthetase[52] (PDB entry 2D7J). Figure 5 shows a backbone superposition of these two structures. Significant differences are found only for residues in β-strands V−VIII, which are shorter in the solution structures. Additionally, residues 68−70, which are present in a 3_{10}-helix in the crystal structure, exist in a coil-like conformation in the solution structure. These differences could be attributed to the local dynamics. The Mj and Ph GATases are structurally similar to the GATase in *two-domain-type* GMPS.

^{15}N Backbone Dynamics. Figure 6 shows the measured ^{15}N T_1 and T_2 relaxation times for Mj GATase, as a function of residue number. The average values of ^{15}N T_1 and T_2 for GATase polypeptide backbone nitrogen atoms are 0.650 ± 0.03 and 0.089 ± 0.003 s, respectively. The residues in α-helices and β-sheets exhibit a tight distribution of T_1 and T_2 values. This is an indication of well-structured regions and corroborates the calculated solution structure. On the other hand, residues in loop regions show a wider distribution of T_1. The residues present in loops showed a lower than average value of T_2, e.g., G51 and G52.

Using the average values of T_1 and T_2, the average global rotational correlational time τ_c was found to be ∼8.0 ns. The observed value is lower than what one could expect for a 21 kDa molecule (i.e., 10.5 ns).

Biochemical Studies. *Substrate-Liganded ATPPase Is Required for Mj GATase Activity.* Mj GATase, in the absence of the ligand-bound ATPPase subunit, is inactive. In the presence of substrate-liganded ATPPase, viz., Mg^{2+}, ATP, and XMP, Mj GATase shows glutaminase activity. A quantitative estimate of this glutaminase activity is shown in Figure 7a. Figure 7b shows the one-dimensional NMR spectra of the conversion of XMP to GMP as a function of time. The resonance lines at 5.9 and 5.92 ppm and those at 8.12 and 8.18 ppm correspond to the H1′ and H8 protons of XMP and GMP, respectively. The resonance line at 6.35 ppm corresponds to that of amino protons of GMP. The decrease in the intensity of resonance lines of XMP with a concomitant increase in the intensity of resonance lines of GMP is unequivocal proof for the conversion of XMP to GMP. Similar changes in the intensity of resonance lines of ATP and AMP can also be observed. The decrease in the intensity of the resonance lines of glutamine is not apparent because of the large stoichiometric excess of this substrate in the reaction mixture. A similar NMR study of GATase alone shows no discernible decrease in the amount of glutamine as a function of time (data not shown). Mj ATPPase, on the other hand, is catalytically active even in the absence of the GATase subunit. Figure 8 shows that the concentration of XMP (5.90 and 8.12 ppm) remains

dx.doi.org/10.1021/bi400472e | *Biochemistry* 2013, 52, 4308−4323

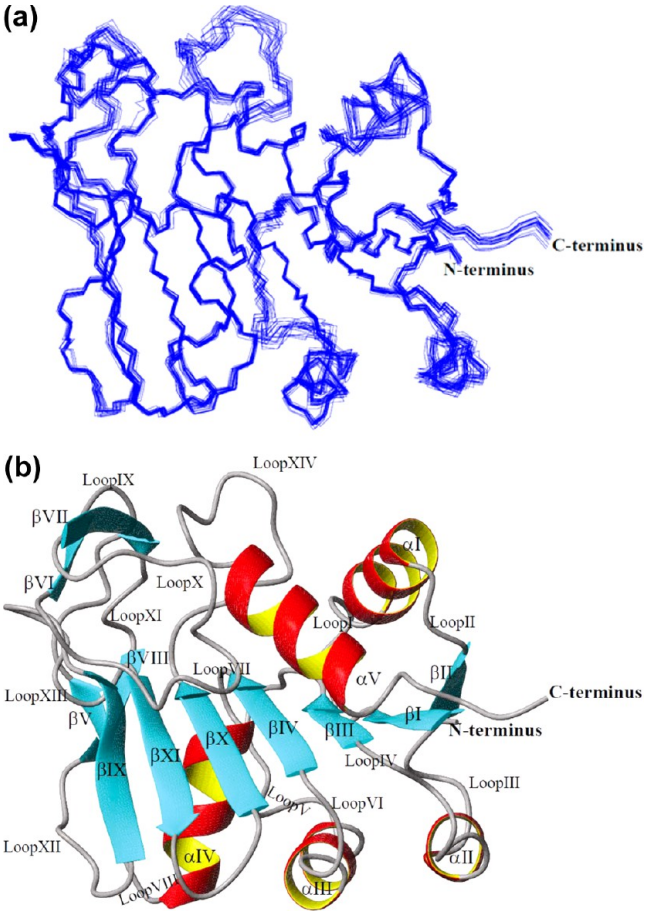

Figure 4. (a) Ensemble of 20 low-energy conformers of the Mj GATase subunit. The structures have been superposed on the backbone (N, C^{α}, and C′ atoms). (b) Ribbon representation of the lowest-energy conformer of the Mj GATase subunit.

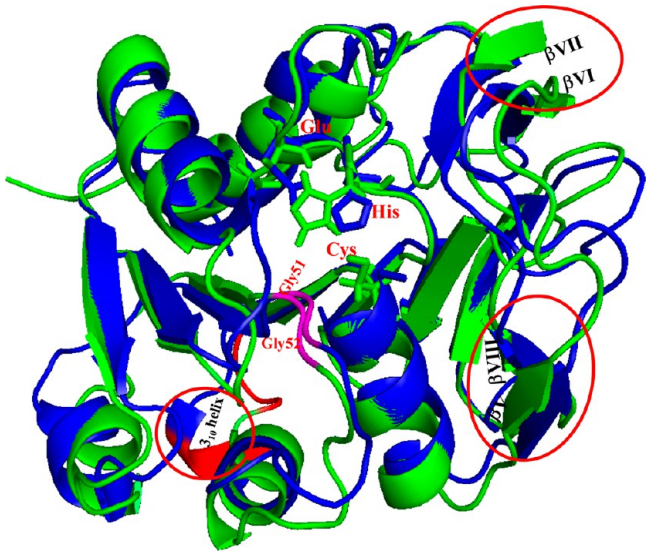

Figure 5. Overlay of the solution NMR representative structure of Mj GATase (green) and the X-ray structure of Ph GATase (PDB entry 2D7J, blue). The shortening of β-sheets observed in the solution structure has been circumscribed by red elipses. Residues 68−70 and residues 51 and 52 are colored red and magenta, respectively. The 3_{10}-helix observed in the X-ray structure of Ph GATase has been circumscribed by a red circle. Catalytic residues Cys, His, and Glu are shown as sticks.

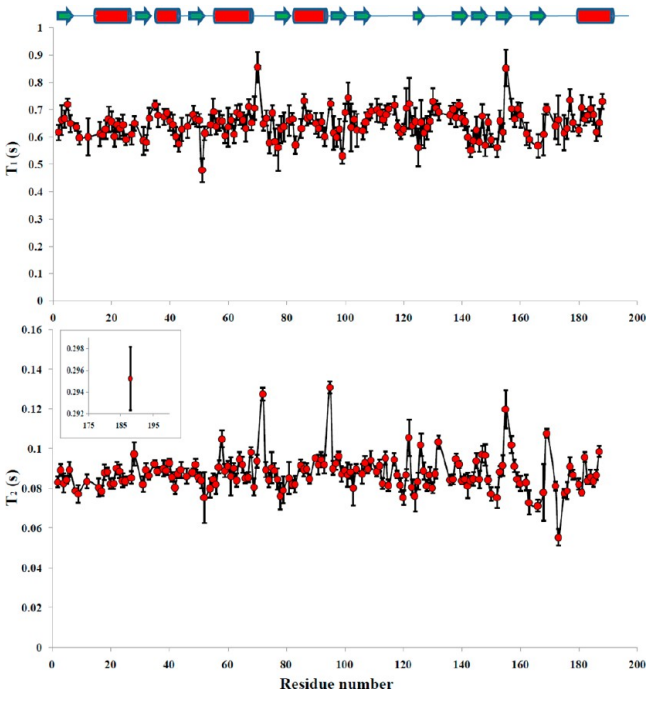

Figure 6. ^{15}N T_1 and T_2 relaxation times, measured on an Agilent 600 NMR spectrometer. The values of T_1 (top) and T_2 (bottom) are plotted as a function of residue number. Shown in the inset of the bottom panel is the T_2 value of C-terminal E188. The secondary structural elements are shown as cylinders (α-helices) and arrows (β-sheets).

unchanged, while that of AMP (8.55 ppm) increases as a function of time.

Stoichiometry of GATase and ATPPase in the GMPS Complex. Figure 9 shows the result of Mj ATPPase titration with varying concentrations of Mj GATase. A maximal GMP synthetase activity was observed at a GATase:ATPPase ratio of 1, indicating the stoichiometry of the functional Mj ATPPase−GATase complex in a functional Mj GMPS is 1:1.

Interaction Studies. *Interaction between GATase and Cofactor Mg^{2+}.* Binding of Mg^{2+} to the Mj GATase subunit was studied by NMR spectroscopy. A concentration-dependent perturbation of chemical shifts was observed for several residues in the protein. An overlay of the HSQC spectra of Mg^{2+}-free GATase and Mg^{2+}-saturated ^{15}N-labeled Mj GATase is shown in Figure S2 of the Supporting Information. Figure 10a shows the chemical shift changes in the HSQC spectra for some of the selected residues that are affected by Mg^{2+} binding. According to Cavanagh et al., "The near continuous change in chemical shift as a function of increasing Mg^{2+} concentration is a clear indication that the protein and metal are in a fast chemical exchange regime on NMR time scale".[42] There were no detectable changes in the spectrum at concentrations of <400 μM and no further change in chemical shift at Mg^{2+} concentrations of >10 mM, indicating that protein had reached saturation.

The absolute value of the deviation in chemical shift, when compared to that of the free protein, is shown in Figure S3 of the Supporting Information. Residues that showed a weighted chemical shift change (Δ) of >0.05 ppm were considered for

dx.doi.org/10.1021/bi400472e | *Biochemistry* 2013, 52, 4308−4323

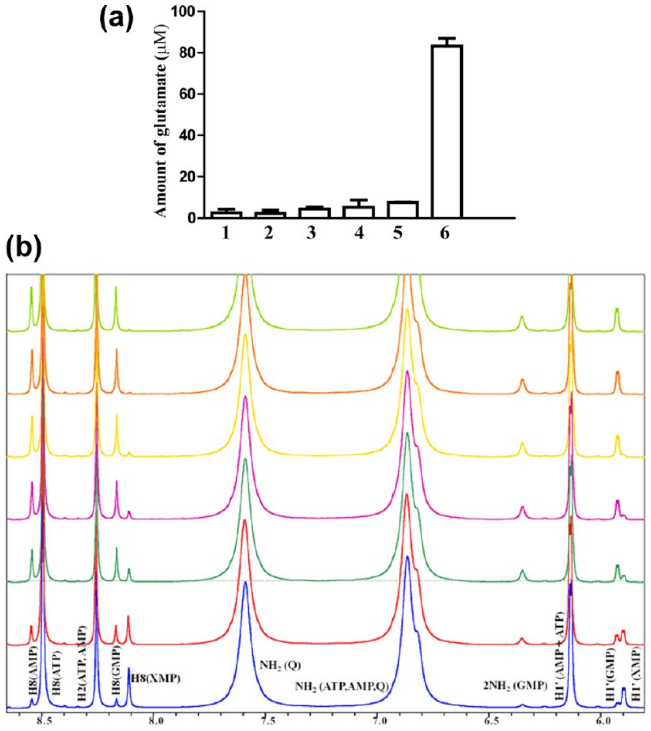

Figure 7. (a) Measurement of Mj GATase activity: (1) GATase and Q, (2) ATPPase and Q, (3) GATase, ATPPase, and Q, (4) GATase, ATPPase, Mg^{2+}, Q, and ATP, (5) GATase, ATPPase, Mg^{2+}, Q, and XMP, and (6) GATase, ATPPase, Mg^{2+}, Q, ATP, and XMP. See the text for details. (b) GMP sythetase activity monitored by NMR. The formation of GMP is accompanied by a concomitant decrease in the XMP concentration. See the text for details.

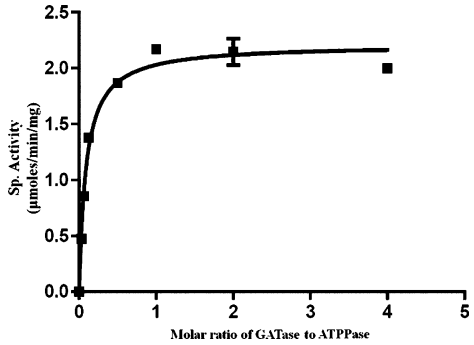

Figure 9. Measurement of Mj GMP synthetase activity for different stoichiometries of GATase and ATPPase. Maximal activity is observed for a 1:1 GATase:ATPPase ratio.

calculation of the dissociation constant. Twelve residues exhibited Δ values of >0.05 ppm. When these residues were mapped on the solution structure of the Mj GATase subunit, all residues showing major chemical shift perturbations were present on one side or face of the structure, around the catalytic residue (Figure 10b). Residues close to the active site, such as H16, G78, H79, S124, H125, D127, and V166, experience significant chemical shift perturbation. Other residues, viz., I5, G9, I28, G88, and A93, also experience measurable perturbation. This could be attributed to changes in conformation induced by Mg^{2+} binding.

The binding curves for the Mg^{2+}–Mj GATase interaction for some of the selected residues are shown in Figure 10c. The dissociation constant, K_d, was calculated using eq 2 and was found to be ∼1 mM. The fact that the K_d is in the millimolar range indicates that the interaction between GATase and Mg^{2+} is very weak and falls in the very fast exchange regime on the NMR time scale. The implications of binding of Mg^{2+} to GATase are discussed below.

Interaction between Mj GATase and ATPPase. *Gel Filtration Chromatography.* The gel filtration studies (*vide*

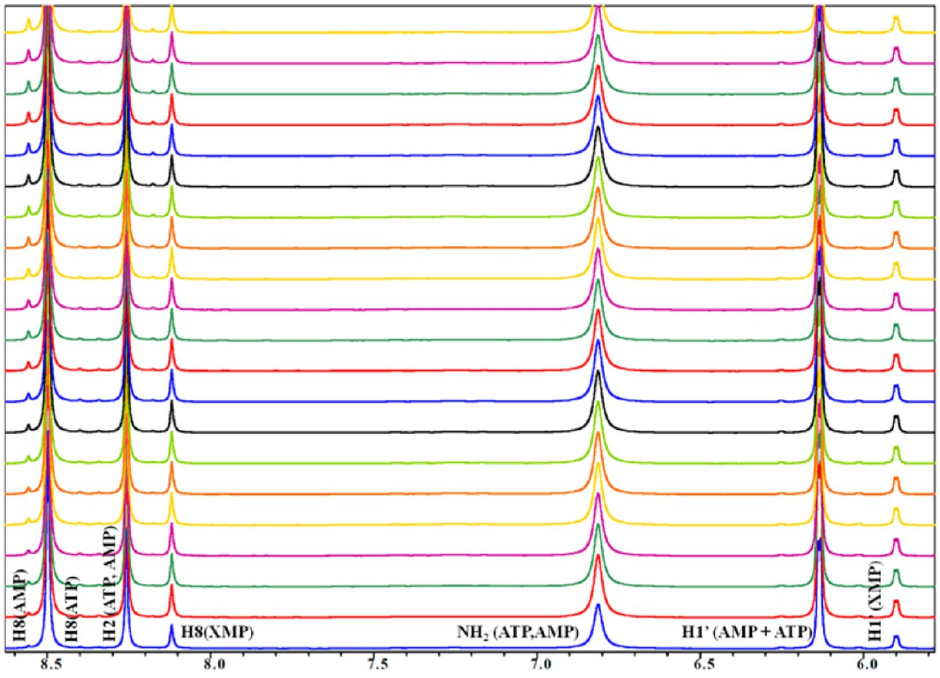

Figure 8. Progress of the reaction independently catalyzed by the Mj ATPPase subunit. The increase in the intensity of the AMP peak as a function of time is visible as the reaction progresses. Note that AMP formation results from the XMP-dependent cleavage of ATP. AMP buildup can be seen clearly by tracking the H8 resonance of AMP.

dx.doi.org/10.1021/bi400472e | *Biochemistry* 2013, 52, 4308–4323

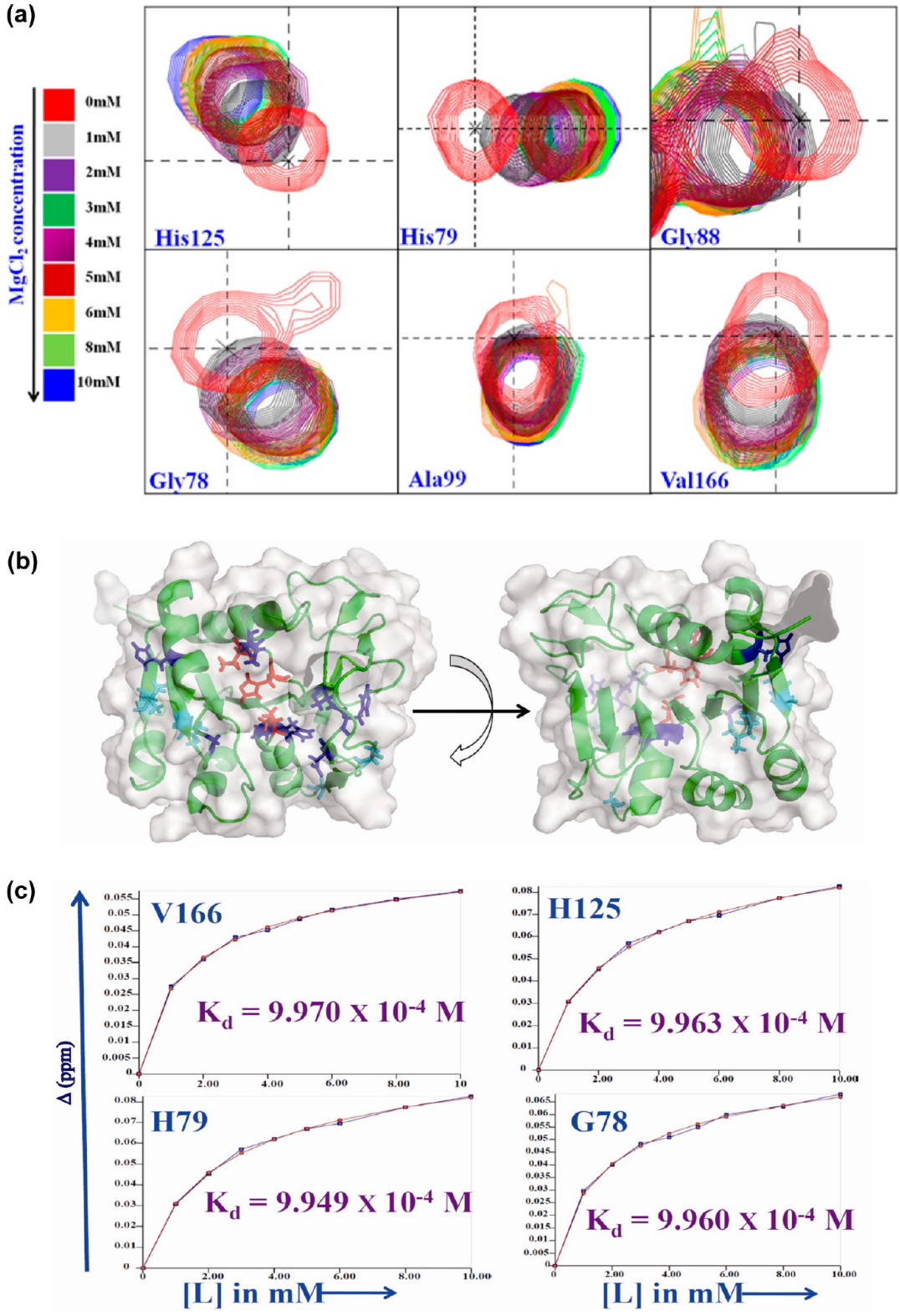

Figure 10. (a) Changes in chemical shifts observed in various $^{1}H-^{15}N$ HSQC spectra of the ^{15}N-labeled MjA GATase subunit, upon titration with varying $MgCl_2$ concentrations. The change in chemical shift is shown with respect to the unbound protein. (b) Cartoon surface representation of the Mg^{2+} binding sites on the Mj GATase structure. The catalytic residues are colored red (stick representation). The residues that bind with Mg^{2+} and are present around the catalytic site are colored blue. The residues colored cyan are those showing significant chemical perturbation caused by conformational changes upon Mg^{2+} binding. (c) Fitting of the titration curve for some of the well-resolved Mj GATase residues.

supra) have shown that Mj GATase exists in solution as a monomer, with a molecular weight of ~21 kDa. Evidence of this also comes from the ^{15}N relaxation studies described above. The gel filtration studies also showed that the Mj ATPPase subunit exists as a dimer with a molecular weight of ~80 kDa. Figure 11a shows the chromatogram of the elution profile of Mj

dx.doi.org/10.1021/bi400472e | *Biochemistry* 2013, 52, 4308−4323

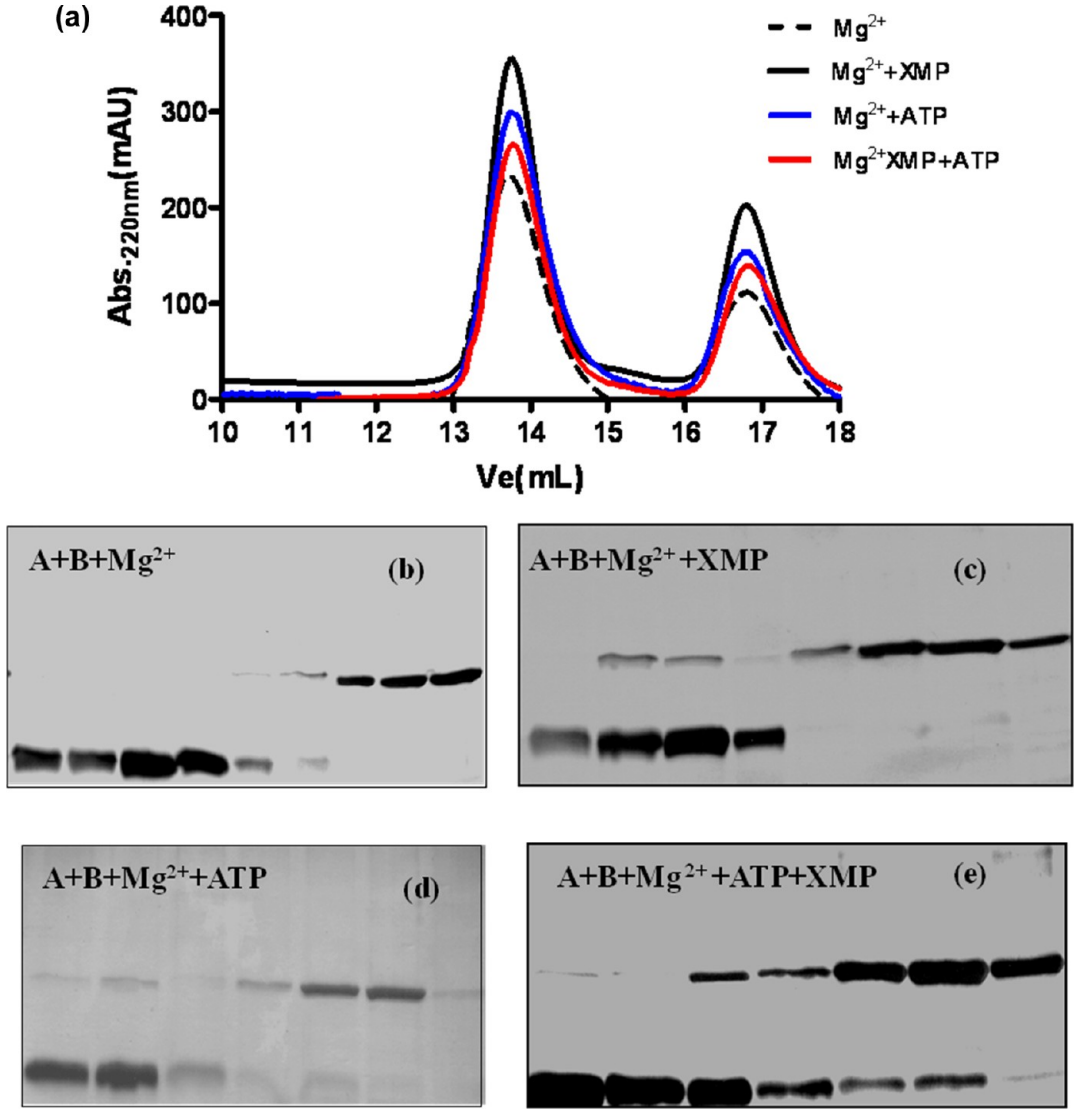

Figure 11. Ligand-mediated association of GATase with ATPPase. (a) Elution profile of Mj GATase and ATPPase on an analytical size-exclusion Superdex 200 column under different conditions, viz., 2 mM $MgCl_2$; 2 mM $MgCl_2$ and 100 μM ATP; 2 mM $MgCl_2$ and 100 μM XMP; 2 mM $MgCl_2$, 100 μM ATP, and 100 μM XMP. (b–e) SDS–PAGE of the protein fractions collected under different conditions indicated by analytical gel filtration. Protein bands were developed by silver staining of the gel.

GATase and ATPPase under different conditions. Under the chromatographic conditions used, the complex should elute as a distinct peak ahead of ATPPase. However, as this peak was absent, fractions of the peak corresponding to ATPPase were examined via SDS–PAGE, and a low level of GATase was seen in the ATPPase fractions (Figure 11b–e). To improve the ratio of ATPPase and GATase co-eluting, a pull-down experiment was conducted. This yielded greater recovery of the protein–protein complex (Figure 12).

NMR Spectroscopic Studies. The one-dimensional proton NMR spectrum of the interaction of the Mj GATase and ATPPase subunits is shown in Figure 13a. An overall broadening of the resonances in Mj GATase can be observed in the spectrum. Broadening of the resonance could arise due to chemical exchange of the components of the complex or due to an increase in the rotational correlation time (τ_c) as a function of the molecular size of the complex. The former would suggest that the complex is in intermediate exchange, while the later would indicate that the complex is in slow exchange. To gain further insight into the interaction between Mj GATase and ATPPase subunits at the atomic level, $^1H-^{15}N$ HSQC spectra of ^{15}N-labeled Mj GATase in the presence of varying concentrations of unlabeled Mj ATPPase and a constant saturating concentration of ATP, Mg^{2+}, and XMP were acquired. Figure 13b shows the ovelay of two $^1H-^{15}N$ HSQC spectra. In the absence of substrates and cofactors, the Mj GATase subunit does not bind to the Mj ATPPase subunit. However, upon addition of $MgCl_2$, ATP, and XMP, a significant reduction in the intensity of the correlation peaks was observed for specific residues in Mj GATase (Figure 13c). The change in intensities for some of the interacting residues with respect to the intensities in the control experiment is shown in Figure 13d and Figure S4 of the Supporting Information. The molecular weight of the Mj GATase–ATPPAse complex is large (~112 kDa), and therefore, the observed overall reduction in intensity could be attributed to the increased molecular weight. The greater than average reduction in intensity observed for specific residues in Mj GATase as a function of the increasing concentration of the Mj ATPPase subunit in presence of all substrates indicates that Mj

dx.doi.org/10.1021/bi400472e | *Biochemistry* 2013, 52, 4308–4323

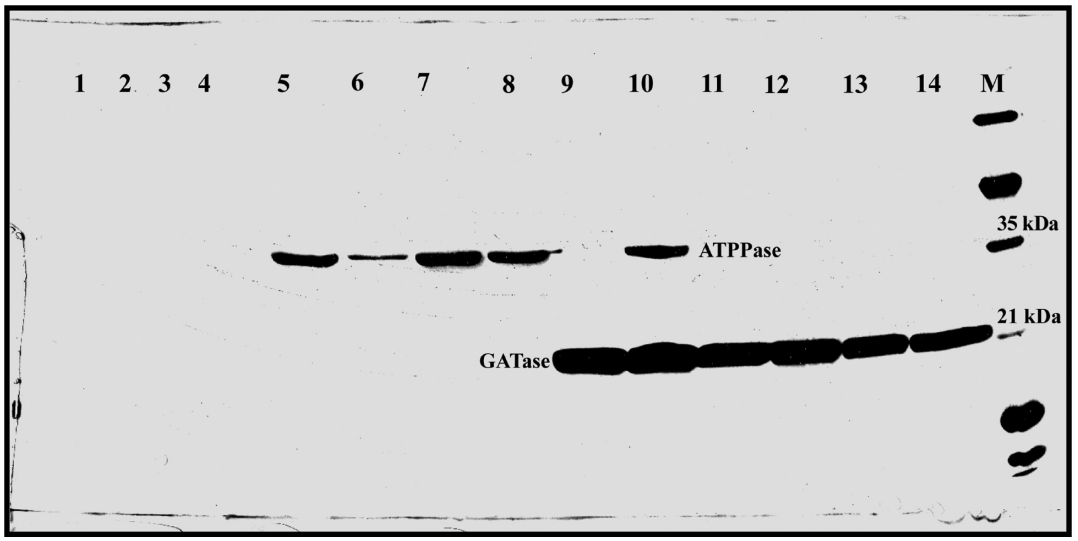

Figure 12. Interaction between Mj GATase and ATPPase subunits: lane 1, GATase flow through (cont); lane 2, GATase flow through (exp); lane 3, GATase wash (cont); lane 4, GATase wash (exp); lane 5, GATase and ATPPase flow through (cont.); lane 6, GATase and ATPPase flow through (exp); lane 7, GATase and ATPPase wash (cont); lane 8, GATase and ATPPase wash (exp); lane 9, elute (cont); lane 10, elute (exp); lane 11, elute fraction 2 (cont); lane 12, elute fraction 2 (exp); lane 13, beads (cont); lane 14, beads (exp). M is the molecular weight marker. Note that (exp) refers to an experiment conducted in the presence of ligands, while (cont.) refers to that conducted in the absence of ligands. Experimental details are as described in Materials and Methods.

GATase and ATPPase are in chemical exchange, between bound and unbound forms, at a rate that is intermediate on the NMR time scale.

A plot of the normalized change in intensity, $\Delta I_{normalized}$, as a function of residue number of the Mj GATase subunit is shown in Figure 14a. In all, 37 residues showed a significant decrease in intensity ($\Delta I_{normalized} > 0.80$) upon Mj ATPPase binding. These residues were identified as those that were directly involved in the interaction between Mj GATase and ATPPase subunits. In addition to these, another set of 27 residues also showed significant decreases in intensity ($0.75 \leq \Delta I_{normalized} \leq 0.80$). The decrease in intensities of these residues is most likely due to secondary effects. The residues of the Mj GATase subunit that are involved in interaction and form the interaction surface are listed in Table 2. When mapped onto the structure of Mj GATase, these residues were found to be concentrated in five regions of the structure (Figure 14b). The residues stretching from V12 to I22 form helix α-1, while the other four stretches of the residues are present in loop V, loop VII, loop XI, and loop XIV around the catalytic triad (C76, H163, and E165). Figure 14c shows the surface representation of the Mj GATase subunit showing residues involved in the interaction. Residues involved in the direct interaction with the Mj ATPPase subunit are colored blue, while the residues involved in the indirect interaction are colored cyan. Interestingly, catalytic residues C76 and H163 also showed changes in intensity of >0.80. We could not evaluate the change in the intensity of E165 because this cross-peak overlaps with V29. This clearly indicates that catalytic residues of Mj GATase also undergo a conformational change upon interacting with the Mj ATPPase subunit. This probably explains why the Mj GATase subunit is inactive in the absence of the ATPPase subunit. Therefore, we surmise that this interaction causes a conformational change, which is transmitted around the catalytic site, leading to the activation of the Mj GATase subunit.

The Complex of GATase and ATPPase Results from a Weak Interaction. The stability of the Mj GATase−ATPPase complex was probed by H−D exchange NMR experiments. Figure S5 of the Supporting Information shows an overlay of HSQC spectra of solutions containing Mj GATase and ATPPase in the absence (red) and presence (blue) of all substrates (induces complexation), both of which were acquired in D_2O. The residues in α-1 are slow to exchange in both cases, which is not surprising as the backbone amide protons are hydrogen-bonded. However, residues in loops exchange rapidly with D_2O. Thus, the residues in the loop regions are not protected in the complex, and it is safe to conclude that the interaction between Mj GATase and ATPPase subunits is a transient one and does not result in a stable complex.

DISCUSSION

The biosynthesis of GMP in most of the archaea is catalyzed by a *two-subunit-type* GMPS enzyme. On the other hand, higher organisms, including eubacteria, possess a multidomain GMPS, which probably arose through gene fusion. While much is known about the structure and kinetic and enzymatic properties of the *two-domain-type* GMPS, the *two-subunit-type* is less well characterized. Here we have determined the three-dimensional solution NMR structure of the GATase subunit of a *two-subunit-type* GMPS from *M. jannaschii.* The structure shows that the molecule is compact and exhibits an $\alpha+\beta$ fold. The calculated average global correlation time for the Mj GATase subunit was almost 2.5 ns smaller than the expected average global correlation time. This strongly indicates that the molecule is rigid and tightly packed and tumbles isotropically in solution. H−D exchange studies showed that almost 40% of the Mj GATase residues either are involved in hydrogen bonding in secondary structure or are buried inside the protein core.

During the course of our studies, we had observed that the optimal activity of GMPS was achieved only under conditions in which the Mg^{2+} was present at a concentration that was significantly higher than that essential for charge stabilization of ATP. Similar observations have also been made in the case of

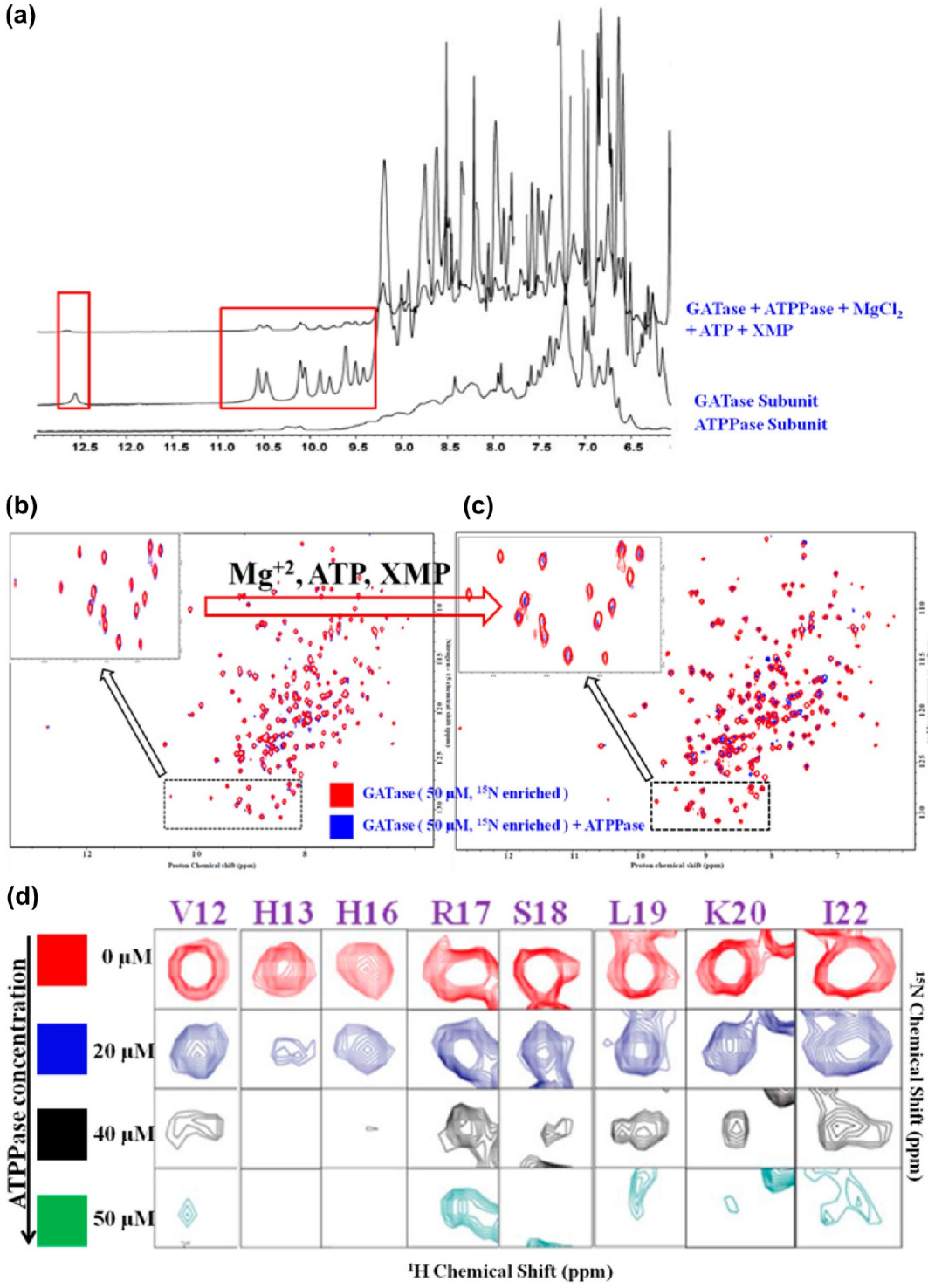

Figure 13. (a) Overlay of ^{1}H one-dimensional spectra of GATase, ATPPase, and GATase, ATPPase in the presence of all substrates. The observed line broadening is highlighted in red rectangles. (b) Overlay of two-dimensional ^{1}H−^{15}N spectra of the ^{15}N-labeled Mj GATase subunit. The red and blue spectra represent the spectra of GATase in the absence and presence of the ATPPase subunit, respectively. Both of the spectra were acquired in absence of substrates. (c) Overlay of two-dimensional ^{1}H−^{15}N spectra of the ^{15}N-labeled Mj GATase subunit. The red spectrum represents the GATase spectrum in the presence of the unbound ATPPase subunit. The blue spectrum represents the GATase spectrum in the presence of ligand-bound ATPPase. Shown in the inset is a decrease in intensity upon GATase−ATPPase interaction. (d) Decrease in intensity of ^{1}H−^{15}N correlation peaks of the ^{15}N-labeled GATase subunit as a function of ATPPase concentration. All spectra were acquired in the presence of a constant saturating substrate concentration. See the text for details.

the *two-domain-type* GMPS from *P. falciparum*[16] and human GMPS.[19] Our titration data, for the first time, showed that magnesium interacts with the Mj GATase subunit in a site specific manner. The residues that are perturbed in chemical shift due to interaction with Mg^{2+} lie on one face of the molecule (Figure 10c) and form a ring around the catalytic site. Figure 15 shows the electrostatic surface potential for Mj GATase. The interaction between Mg^{2+} and Mj GATase is not

dx.doi.org/10.1021/bi400472e | *Biochemistry* 2013, 52, 4308−4323

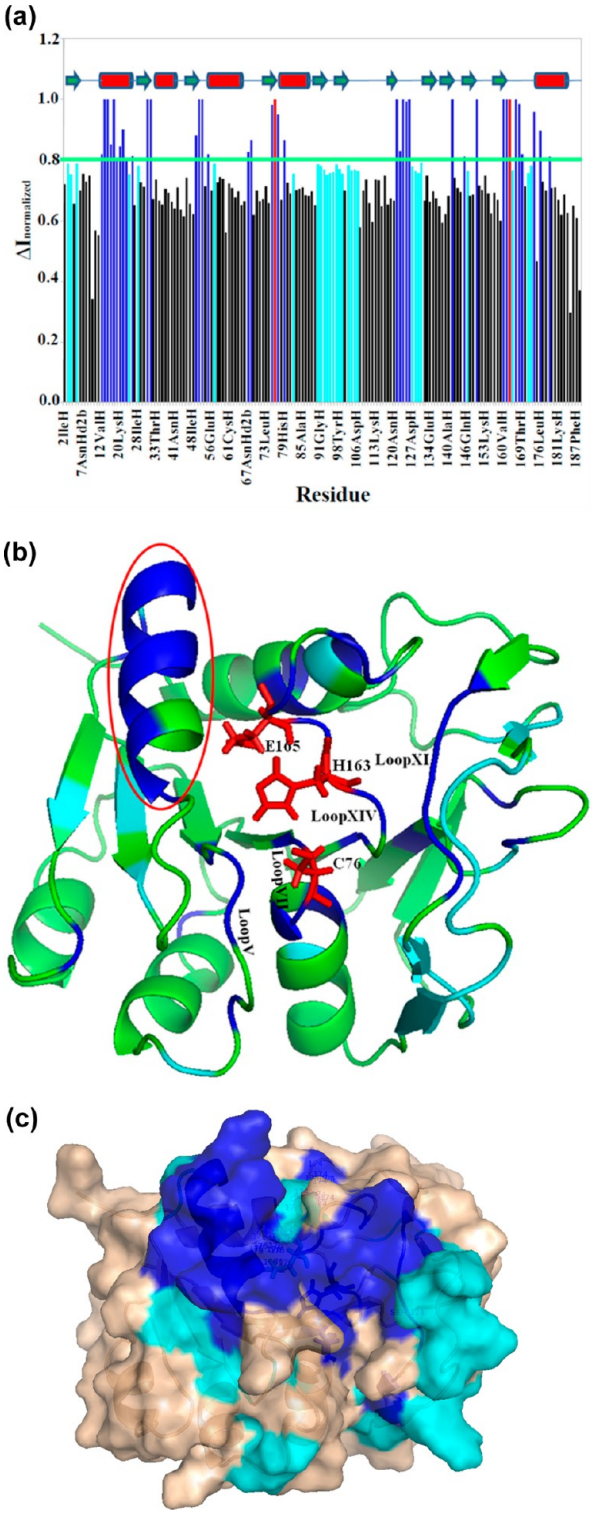

Figure 14. (a) Plot of the normalized change in intensity as a function of residue number of the Mj GATase subunit. The residues showing $\Delta I_{normalized}$ values of >0.80 and $\Delta I_{normalized}$ from 0.75 to 0.80 are colored blue and cyan, respectively. The catalytic residues are colored red. (b) Cartoon representation of the Mj GATase subunit showing ATPPase interaction sites. The catalytic residues are colored red (stick representation). The residues involved in the direct interaction are colored blue, while those involved in the indirect interaction are colored cyan. The positively charged α-helix is highlighted with a red ellipse. (c) Surface representation of the Mj GATase subunit, showing the interaction surface between two subunits.

a case of a nonspecific electrostatically driven interaction. This is supported by the fact that several other negatively charged regions, which are present on the surface of Mj GATase, are unperturbed in the presence of Mg^{2+}. For instance, the surface of helix II is highly negatively charged (four of six residues are negatively charged). However, no change in chemical shift for the residues in helix II was observed upon titration with Mg^{2+}, indicating that the metal−protein interaction is a highly specific one. The high value of the dissociation constant indicates that this is a weak interaction. In the case of human and Pf GMPS, the site of Mg^{2+} binding is unknown.

The mechanism by which ammonia is channeled from the GATase to the ATPPase is complex and poorly understood. Structural studies of *two-domain-type* GMPS do not show a clear conduit for the passage of ammonia from one domain to the other. The structural basis for subunit association in *two-subunit-type* GMPS's is not known. Using high-resolution NMR spectroscopic methods, we have also identified the residues on Mj GATase that are responsible for interaction with the ATPPase subunit. There are eight residues on Mj GATase that are common to the interaction with Mg^{2+} and ATPPase. These residues showed chemical shift perturbation upon Mg^{2+} binding as well as a reduction in intensity upon interaction with the ATPPase subunit. Though the exact role of Mg^{2+} is not known, the fact that a significant number of residues are involved in Mg^{2+} binding and that these residues are also involved in interaction with ATPPase indicates that Mg^{2+} binding must play an important role. Because Mg^{2+} can bind to the GATase subunit independently, one may postulate that Mg^{2+} binding may play an important role in charge stabilization of the GATase−ATPPase complex.

It is important to note that the Mj GATase−ATPPase interaction takes place only in the presence of substrates. The Mj GATase−ATPPase complex undergoes exchange that is intermediate on the NMR time scale. Evidence of this comes from the fact that correlation peaks of the ^{15}N-labeled Mj GATase subunit showed neither chemical shift perturbations nor the appearance of new correlation peaks with an increasing concentration of the ATPPase subunit. This rules out the possibility of a fast chemical exchange regime or a slow exchange chemical regime, respectively. Instead, a significant line broadening effect was observed as a function of an increasing concentration of ATPPase. This could be attributed to the intermediate chemical exchange between two subunits in the Mj GATase−ATPPase complex, on the NMR time scale. The intermediate chemical exchange regime is characterized by complete broadening of resonances at approximately half of the saturating concentrations of the ligand and then reappears, probably at slightly different chemical shifts, at much higher concentrations of the ligand.[42] Given the fact that the apparent molecular weight of Mj GATase increases from 21 to 112 kDa, upon complexation with the ATPPase subunit, it is expected that there will be some contribution to the observed line width from the increased rotational correlation time.

Most of the studies of GMPS have shown that glutaminase activity is regulated by interaction between GATase and ATPPase subunits. However, a recent study of IGPS[53,54] from *Thermotoga maritima*, a *two-subunit-type* amidotransferase, has shown that indeed GAT is independently active and the absence of constitutive activity is due to the presence of a plug in the channel in the GAT domain. Removal of the plug results in constitutive activity. We therefore checked in Mj GATase for such an independent activity using large equimolar quantities of

dx.doi.org/10.1021/bi400472e | *Biochemistry* 2013, 52, 4308−4323

Table 2

directly interacting residues	V12, H13, H16, R17, S18, L19, K20, Y21, I22, V24, N31 (side chain), L49, G51, G52, I55, N67 (side chain), I75, C76, L77, H79, A121, W122, A123, S124, H125, H141, C145, A149, V160, F162, H163, V166, H168, T169, E174, L176, N178 (side chain)
indirectly interacting residues	V3, I4, D6, G23, I28, K57, I82, V90, G91, R92, A93, A95, E96, E97, Y98, A99, K102, V103, Y104, D106, D127, E128, V129, K130, Q146, E165, N173 (side chain)

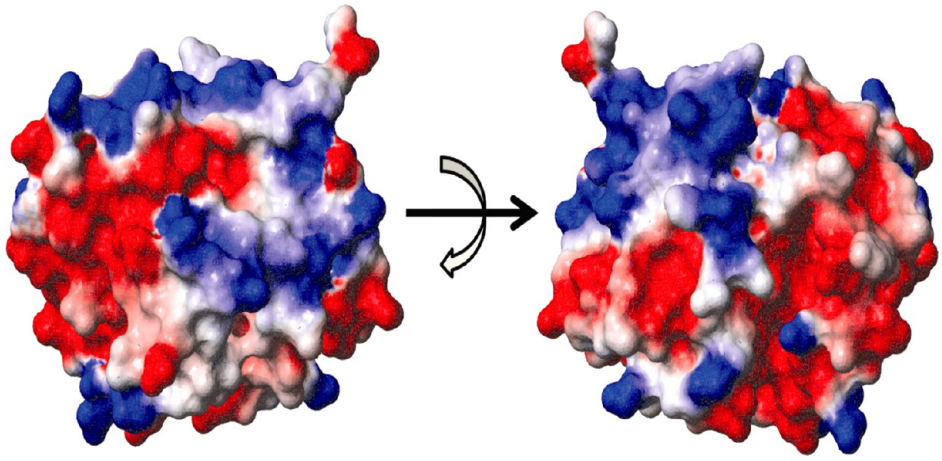

Figure 15. Surface potential representation of the Mj GATase structure. Large negatively charged patches can be seen on both sides of the Mj GATase structure.

enzyme and glutamine. No measurable activity was observed when GATase and glutamine were incubated at either 22 or 70 °C. It should be noted that under our assay condition, glutamate concentrations as low as 5 μM can be reliably measured. Thus, it is safe to conclude that Mj GATase has no activity and that its activity seems to be tightly regulated. Our NMR studies have shown that catalytic residues C76 and H163 also undergo conformational changes upon Mj GATase–ATPPase interaction. The role of catalytic cysteine in the GATase domain has been known to be very important.[20,21,55,56] This is a strong indication that there are conformational changes at the catalytic site upon interaction with ATPPase and that these changes could lead to activation of the Mj GATase subunit.

Hydrogen–deuterium exchange data provide valuable information about the physical environment of exchangeable protons, i.e., whether they are present in regions of the molecule that are solvent inaccessible and/or are strongly hydrogen bonded. Residues that are solvent-exposed often become protected from solvent when they are part of an intermolecular interface. The rate at which these protons undergo solvent exchange is a measure of the strength of association, particularly when the interaction occurs between large molecules. The rates of exchange of solvent-exposed residues in Mj GATase in the presence and absence of ATPPase were nearly identical. This suggests that the complex is not in slow exchange but rather exchanges on a time scale that is intermediate to fast.

The residues involved in the interaction with ATPPase are those that are present in helix I and in loops V, VII, XI, and XIV. Except for helix I, the residues in the loops are present around the catalytic site. The residues in helix I are V12, H13, R14, V15, H16, R17, S18, L19, K20, Y21, and I22. A survey of protein–protein interaction surfaces has shown that Trp, Arg, and Tyr predominate and these are considered "hot spots". In addition, His, Ile, Lys, Leu, and Met are also found in high proportions. Helix I is well represented by these hot spot residues. It has been shown that protein–protein interaction surfaces are generally uneven and consist of rigid and nonrigid structural elements. Furthermore, ~65% of the core interface is formed by rigid residues.[57−59] In our case, a tight distribution of T_1 and T_2 values for residues V12–I22 indicates that this helix is rigid. Additionally, the preponderance of positively charged residues in helix I suggests that electrostatic interactions may play a very important role in steering complex formation, which could be stabilized by salt bridges.[60]

In conclusion, we have determined the solution NMR structure of the Mj GATase subunit and have shown its interaction with $MgCl_2$. Most importantly, we have identified the specific residues on Mj GATase that are responsible for interaction with the ATPPase subunit. The interaction between these subunits in a *two-subunit-type* GMPS has not been established earlier.

The interaction between Mj GATase and Mg^{2+} falls in the fast chemical exchange regime on the NMR time scale. The interaction between Mj GATase and ATPPase subunits falls in the intermediate chemical exchange regime on the NMR time scale. This implies that ammonia channeling occurs at a rate that is fast compared to the rate of exchange of the protein–protein complex.

■ ASSOCIATED CONTENT

Supporting Information

Figures providing corroborative evidence of the data provided here. This material is available free of charge via the Internet at http://pubs.acs.org.

Accession Codes

The structural coordinates for the 20 low-energy structures of Mj GATase have been deposited in the Protein Data Bank as entry 2LXN. The chemical shift assignments for Mj GATase have been deposited in the Biological Magnetic Resonance Bank as entry 17935.

AUTHOR INFORMATION

Corresponding Author

*Address: 207 Molecular Biophysics Unit, Indian Institute of Science, Bangalore 560012, Karnataka, India. E-mail: sidd@mbu.iisc.ernet.in. Telephone: 918022932839. Fax: 918023600535.

Funding

We thank the Department of Science and Technology and the Department of Biotechnology, Government of India, for the NMR and mass spectrometric facilities at the Indian Institute of Science. H.B. acknowledges the Department of Biotechnology and Department of Science and Technology, Government of India, for funding. R.A. is grateful to the Indian Institute of Science for a doctoral fellowship. S.K. was a recipient of CSIR Junior Research and Senior Research fellowships.

Notes

The authors declare no competing financial interest.

ABBREVIATIONS

ATPPase, ATP pyrophosphatase; DSS, sodium 4,4-dimethyl-4-silapentanesulfonate; ESI-MS, electrospray ionization mass spectrometry; GAT, glutamine-dependent amidotransferase; GDH, glutamate dehydrogenase; GATase, glutamine amidotransferase; GMP, guanosine monophosphate; GMPS, guanosine monophosphate synthetase; HSQC, heteronuclear single-quantum coherence; IGPS, imidazole glycerolphosphate synthase; MALDI-TOF, matrix-assisted laser desorption ionization time of flight; Mj GATase, *M. jannaschii* GATase; Mj GMPS, *M. jannaschii* GMPS; NAD, nicotinamide adenine dinucleotide; NMR, nuclear magnetic resonance; NOE, nuclear Overhauser effect; NOESY, nuclear Overhauser effect spectroscopy; Ph, *P. horikoshii*; XMP, xanthosine monophosphate; rmsd, root-mean-square deviation.

REFERENCES

(1) Janin, J., and Wodak, S. J. (2002) Protein molecules and protein-protein interactions. *Adv. Protein Chem. 61*, 1−8.

(2) Jones, S., and Thornton, J. M. (1996) Principles of protein-protein interactions. *Proc. Natl. Acad. Sci. U.S.A. 93*, 13−20.

(3) Reichman, D., Rahat, O., Cohen, M., Neuvirth, H., and Schreiber, G. (2007) Molecular architecture of protein-protein binding sites. *Curr. Opin. Struct. Biol. 17*, 67−76.

(4) Zalkin, H., and Murphy, T. (1975) Utilization of ammonia for tryptophan synthesis. *Biochem. Biophys. Res. Commun. 67*, 1370−1377.

(5) Massiere, F., and Badet-Denisot, M. A. (1998) The mechanism of glutamine-dependent amidotransferases. *Cell. Mol. Life Sci. 54*, 205−222.

(6) Schendel, F. J., Mueller, E., Stubbe, J., Shiau, A., and Smith, J. M. (1989) Formylglycinamide ribonucleotide synthetase from *Escherichia coli*: Cloning, sequencing, overproduction, isolation, and characterization. *Biochemistry 28*, 2459−2471.

(7) Zalkin, H. (1993) The amidotransferases. *Adv. Enzymol. Relat. Areas Mol. Biol. 66*, 203−309.

(8) Zalkin, H., and Smith, J. L. (1998) Enzymes using glutamine as an amide donor. *Adv. Enzymol. Relat. Areas Mol. Biol. 72*, 87−144.

(9) Fukuyama, T. T. (1966) Formation of an adenyl xanthosine monophosphate intermediate by xanthosine 5′-phosphate aminase and its inhibition by psicofuranine. *J. Biol. Chem. 241*, 4745−4749.

(10) von der Saal, W., Anderson, P. M., and Villafranca, J. J. (1985) Mechanistic investigations of *Escherichia coli* cytidine-5′-triphosphate synthetase. Detection of an intermediate by positional isotope exchange experiments. *J. Biol. Chem. 260*, 5343−5350.

(11) von der Saal, W., Crysler, C. S., and Villafranca, J. J. (1985) Positional isotope exchange and kinetic experiments with *Escherichia coli* guanosine-5′-monophosphate synthetase. *Biochemistry 24*, 5343−5350.

(12) Tesmer, J. J., Klem, T. J., Deras, M. L., Davisson, V. J., and Smith, J. L. (1996) The crystal structure of GMP synthetase reveals a novel catalytic triad and is a structural paradigm for two enzyme families. *Nat. Struct. Biol. 3*, 74−86.

(13) Mouilleron, S., and Golinelli-Pimpaneau, B. (2007) Conformational changes in ammonia-channeling glutamine amidotransferases. *Curr. Opin. Struct. Biol. 17*, 653−664.

(14) Raushel, F. M., Thoden, J. B., and Holden, H. M. (2003) Enzymes with molecular tunnels. *Acc. Chem. Res. 36*, 539−548.

(15) Huang, X., Holden, H. M., and Raushel, F. M. (2001) Channeling of substrates and intermediates in enzyme-catalyzed reactions. *Annu. Rev. Biochem. 70*, 149−180.

(16) Bhat, J. Y., Shastri, B. G., and Balaram, H. (2008) Kinetic and biochemical characterization of *Plasmodium falciparum* GMP synthetase. *Biochem. J. 409*, 263−273.

(17) Bhat, J. Y., Venkatachala, R., and Balaram, H. (2011) Substrate-induced conformational changes in *Plasmodium falciparum* guanosine monophosphate synthetase. *FEBS J. 278*, 3756−3768.

(18) Bhat, J. Y., Venkatachala, R., Singh, K., Gupta, K., Sarma, S. P., and Balaram, H. (2011) Ammonia Channeling in *Plasmodium falciparum* GMP Synthetase: Investigation by NMR Spectroscopy and Biochemical Assays. *Biochemistry 50*, 3346−3356.

(19) Nakamura, J., and Lou, L. (1995) Biochemical characterization of human GMP synthetase. *J. Biol. Chem. 270*, 7347−7353.

(20) Nakamura, J., Straub, K., Wu, J., and Lou, L. (1995) The glutamine hydrolysis function of human GMP synthetase. Identification of an essential active site cysteine. *J. Biol. Chem. 270*, 23450−23455.

(21) Zalkin, H., and Truitt, C. D. (1977) Characterization of the glutamine site of *Escherichia coli* guanosine 5′-monophosphate synthetase. *J. Biol. Chem. 252*, 5431−5436.

(22) Maruoka, S., Horita, S., Lee, W. C., Nagata, K., and Tanokura, M. (2010) Crystal structure of the ATPPase subunit and its substrate-dependent association with the GATase subunit: A novel regulatory mechanism for a two-subunit-type GMP synthetase from *Pyrococcus horikoshii* OT3. *J. Mol. Biol. 395*, 417−429.

(23) Ali, R., Kumar, S., Balaram, H., and Sarma, S. P. (2012) ^{1}H, ^{13}C, ^{15}N assignment and secondary structure determination of glutamine amido transferase subunit of gaunosine monophosphate synthetase from *Methanocaldococcus jannaschii*. *Biomol. NMR Assignments 6*, 193−196.

(24) Muchmore, D. C., McIntosh, L. P., Russell, C. B., Anderson, D. E., and Dahlquist, F. W. (1989) Expression and nitrogen-15 labeling of proteins for proton and nitrogen-15 nuclear magnetic resonance. *Methods Enzymol. 177*, 44−73.

(25) Patel, N., Moyed, H. S., and Kane, J. F. (1977) Properties of xanthosine-5′-monophosphate amidotransferase from *Escherichia coli*. *Arch. Biochem. Biophys. 178*, 652−661.

(26) Moyed, H. S., and Magasanik, B. (1957) Enzymes essential for the biosynthesis of nucleic acid guanine; xanthosine 5′-phosphate aminase of *Aerobacter aerogenes*. *J. Biol. Chem. 226*, 351−363.

(27) Mori, S., Abeygunawardana, C., Johnson, M. O., and van Zijl, P. C. (1995) Improved sensitivity of HSQC spectra of exchanging protons at short interscan delays using a new fast HSQC (FHSQC) detection scheme that avoids water saturation. *J. Magn. Reson., Ser. B 108*, 94−98.

(28) Piotto, M., Saudek, V., and Sklenar, V. (1992) Gradient-tailored excitation for single-quantum NMR spectroscopy of aqueous solutions. *J. Biomol. NMR 2*, 661−665.

(29) Marion, D., Driscoll, P. C., Kay, L. E., Wingfield, P. T., Bax, A., Gronenborn, A. M., and Clore, G. M. (1989) Overcoming the overlap problem in the assignment of ^{1}H NMR spectra of larger proteins by use of three-dimensional heteronuclear ^{1}H-^{15}N Hartmann-Hahn-multiple quantum coherence and nuclear Overhauser-multiple quantum coherence spectroscopy: Application to interleukin 1β. *Biochemistry 28*, 6150−6156.

(30) Farrow, N. A., Muhandiram, R., Singer, A. U., Pascal, S. M., Kay, C. M., Gish, G., Shoelson, S. E., Pawson, T., Forman-Kay, J. D., and Kay, L. E. (1994) Backbone dynamics of a free and phosphopeptide-complexed Src homology 2 domain studied by ^{15}N NMR relaxation. *Biochemistry 33*, 5984−6003.
(31) Farrow, N. A., Zhang, O., Forman-Kay, J. D., and Kay, L. E. (1994) A heteronuclear correlation experiment for simultaneous determination of ^{15}N longitudinal decay and chemical exchange rates of systems in slow equilibrium. *J. Biomol. NMR 4*, 727−734.
(32) Vranken, W. F., Boucher, W., Stevens, T. J., Fogh, R. H., Pajon, A., Llinas, M., Ulrich, E. L., Markley, J. L., Ionides, J., and Laue, E. D. (2005) The CCPN data model for NMR spectroscopy: Development of a software pipeline. *Proteins 59*, 687−696.
(33) Kay, L. E., Torchia, D. A., and Bax, A. (1989) Backbone Dynamics of Proteins As Studied by ^{15}N Inverse Detected Heteronuclear NMR Spectroscopy: Application to Staphylococcal Nuclease. *Biochemistry 28*, 8972−8979.
(34) Delaglio, F., Grzesiek, S., Vuister, G. W., Zhu, G., Pfeifer, J., and Bax, A. (1995) NMRPipe: A multidimensional spectral processing system based on UNIX pipes. *J. Biomol. NMR 6*, 277−293.
(35) Shen, Y., Delaglio, F., Cornilescu, G., and Bax, A. (2009) TALOS$^+$: A hybrid method for predicting protein backbone torsion angles from NMR chemical shifts. *J. Biomol. NMR 44*, 213−223.
(36) Guntert, P. (1998) Structure calculation of biological macromolecules from NMR data. *Q. Rev. Biophys. 31*, 145−237.
(37) Guntert, P., Billeter, M., Ohlenschlager, O., Brown, L. R., and Wuthrich, K. (1998) Conformational analysis of protein and nucleic acid fragments with a new grid search algorithm FOUND. *J. Biomol. NMR 12*, 543−548.
(38) Koradi, R., Billeter, M., and Wuthrich, K. (1996) MOLMOL: A program for display and analysis of macromolecular structures. *J. Mol. Graphics 14*, 29−32 , 51−55.
(39) Bhattacharya, A., Tejero, R., and Montelione, G. T. (2007) Evaluating protein structures determined by structural genomics consortia. *Proteins 66*, 778−795.
(40) Holm, L., and Rosenstrom, P. (2010) Dali server: Conservation mapping in 3D. *Nucleic Acids Res. 38*, W545−W549.
(41) *The PyMOL Molecular Graphics System*, version 1.3r1 (2010) Schrodinger, LLC, New York.
(42) Cavanagh, J., Fairbrother, W. J., Palmer, A. G. I., Rance, M., and Skelton, N. J. (2007) *Protein NMR Spectroscopy: Principles and Practice*, 2nd ed., Elsevier Academic Press, Amsterdam.
(43) Fielding, L. (2003) NMR methods for the determination of protein-ligand dissociation constants. *Curr. Top. Med. Chem. 3*, 39−53.
(44) Rajagopal, P., Waygood, E. B., Reizer, J., Saier, M. H., Jr., and Klevit, R. E. (1997) Demonstration of protein-protein interaction specificity by NMR chemical shift mapping. *Protein Sci. 6*, 2624−2627.
(45) Schmiedeskamp, M., Rajagopal, P., and Klevit, R. E. (1997) NMR chemical shift perturbation mapping of DNA binding by a zinc-finger domain from the yeast transcription factor ADR1. *Protein Sci. 6*, 1835−1848.
(46) Vaynberg, J., and Qin, J. (2006) Weak protein-protein interactions as probed by NMR spectroscopy. *Trends Biotechnol. 24*, 22−27.
(47) Zuiderweg, E. R. (2002) Mapping protein-protein interactions in solution by NMR spectroscopy. *Biochemistry 41*, 1−7.
(48) Yokogawa, M., Kobashigawa, Y., Yoshida, N., Ogura, K., Harada, K., and Inagaki, F. (2012) NMR Analyses of the Interaction between the FYVE Domain of Early Endosome Antigen 1 (EEA1) and Phosphoinositide Embedded in a Lipid Bilayer. *J. Biol. Chem. 287*, 34936−34945.
(49) Ramachandran, G. N., Ramakrishnan, C., and Sasisekharan, V. (1963) Stereochemistry of polypeptide chain configurations. *J. Mol. Biol. 7*, 95−99.
(50) Ramachandran, G. N., and Sasiskharan, V. (1968) Conformation of polypeptides and proteins. *Adv. Protein Chem. 23*, 283−437.
(51) Nardini, M., and Dijkstra, B. W. (1999) α/β hydrolase fold enzymes: The family keeps growing. *Curr. Opin. Struct. Biol. 9*, 732−737.
(52) Maruoka, S., Lee, W. C., Kamo, M., Kudo, N., Nagata, K., and Tanokura, M. (2005) Crystal structure of glutamine amidotransferase from *Pyrococus horikoshii* OT3. *Proc. Jpn. Acad. 81*, 459−462.
(53) List, F., Bocola, M., Haeger, M. C., and Sterner, R. (2012) Constitutively active glutaminase variants provide insight into the activation mechanism of anthranilate synthase. *Biochemistry 51*, 2812−2818.
(54) List, F., Vega, M. C., Razeto, A., Hager, M. C., Sterner, R., and Wilmanns, M. (2012) Catalysis uncoupling in a glutamine amidotransferase bienzyme by unblocking the glutaminase active site. *Chem. Biol. 19*, 1589−1599.
(55) Abbott, J. L., Newell, J. M., Lightcap, C. M., Olanich, M. E., Loughlin, D. T., Weller, M. A., Lam, G., Pollack, S., and Patton, W. A. (2006) The effects of removing the GAT domain from *E. coli* GMP synthetase. *Protein J. 25*, 483−491.
(56) Chittur, S. V., Klem, T. J., Shafer, C. M., and Davisson, V. J. (2001) Mechanism for acivicin inactivation of triad glutamine amidotransferases. *Biochemistry 40*, 876−887.
(57) Reichman, D., Cohen, M., Abramovich, R., Dym, O., Strynadka, N. C., and Schreiber, G. (2007) Binding hot spots in the TEM1-BL1P interface in light of its modular architecture. *J. Mol. Biol. 365*, 663−679.
(58) Reichmann, D., Rahat, O., Albeck, S., Meged, R., Dym, O., and Schreiber, G. (2005) The modular architecture of protein-protein binding interfaces. *Proc. Natl. Acad. Sci. U.S.A. 102*, 57−62.
(59) Swapna, L. S., Bhaskara, R. M., Sharma, J., and Srinivasan, N. (2012) Roles of residues in the interface of transient protein-protein complexes before complexation. *Sci. Rep. 2*, 334.
(60) Sheinerman, F. B., Norel, R., and Honig, B. (2000) Electrostatic aspects of protein-protein interactions. *Curr. Opin. Struct. Biol. 10*, 153−159.